

FIBROSIS

Long noncoding RNA *lnc-TSI* inhibits renal fibrogenesis by negatively regulating the TGF- β /Smad3 pathway

Peng Wang^{1*}, Man-Li Luo^{2*}, Erwei Song², Zhanmei Zhou¹, Tongtong Ma¹, Jun Wang¹, Nan Jia¹, Guobao Wang¹, Sheng Nie¹, Youhua Liu¹, FanFan Hou^{1†}

Copyright © 2018
The Authors, some
rights reserved;
exclusive licensee
American Association
for the Advancement
of Science. No claim
to original U.S.
Government Works

Transforming growth factor- β (TGF- β) is a well-established central mediator of renal fibrosis, a common outcome of almost all progressive chronic kidney diseases. Here, we identified a poorly conserved and kidney-enriched long noncoding RNA in TGF- β 1-stimulated human tubular epithelial cells and fibrotic kidneys, which we termed TGF- β /Smad3-interacting long noncoding RNA (*lnc-TSI*). *lnc-TSI* was transcriptionally regulated by Smad3 and specifically inhibited TGF- β -induced Smad3 phosphorylation and downstream profibrotic gene expression. *lnc-TSI* acted by binding with the MH2 domain of Smad3, blocking the interaction of Smad3 with TGF- β receptor I independent of Smad7. Delivery of human *lnc-TSI* into unilateral ureteral obstruction (UUO) mice, a well-established model of renal fibrosis, inhibited phosphorylation of Smad3 in the kidney and attenuated renal fibrosis. In a cohort of 58 patients with biopsy-confirmed IgA nephropathy (IgAN), *lnc-TSI* renal expression negatively correlated with the renal fibrosis index ($r = -0.56$, $P < 0.001$) after adjusting for cofounders. In a longitudinal study, 32 IgAN patients with low expression of renal *lnc-TSI* at initial biopsy had more pronounced increases in their renal fibrosis index and experienced stronger declines in renal function at repeat biopsy at a mean of 48 months of follow-up. These data suggest that *lnc-TSI* reduced renal fibrogenesis through negative regulation of the TGF- β /Smad pathway.

INTRODUCTION

Progressive forms of chronic kidney disease are invariably associated with tubulointerstitial fibrosis (TIF), resulting in an ongoing loss of normal tissue structure and renal function that can lead to end-stage renal disease (1–3). It is well established that progressive TIF is exacerbated by multiple mediators including growth factors, metabolic toxins, and stress molecules (4–6). Among them, transforming growth factor- β (TGF- β 1) has been recognized as a key mediator in the pathogenesis of TIF (2, 7, 8).

TGF- β 1 has a broad spectrum of biological actions in a wide variety of cell types, including renal tubular epithelial cells (TECs) (9, 10). TGF- β 1 initiates its cellular actions across multiple cell types by binding with the TGF- β type II receptor, which activates the TGF- β type I receptor (T β RI), resulting in the phosphorylation of Smad2/3 (11, 12). The activated Smad complex then translocates into the nucleus and regulates the transcription of human profibrotic genes such as type I collagen (*COL1A1*) (13), α -smooth muscle actin (*α SMA*) (14), and Snail (*SNAIL1*) (15).

Although Smad3 has been suggested to be a key transcription factor activated in response to many fibrogenic mediators, knockout of *SMAD3* can cause autoimmune disease (16, 17). No specific treatment is currently available to attenuate renal fibrogenesis and preserve organ function. Therefore, alternative approaches to inhibiting the TGF- β /Smad pathway could be of importance in suppressing renal fibrosis without impairing the immune system.

Long noncoding RNAs (lncRNAs) are a heterogeneous class of long [>200 nucleotides (nt)] transcripts without protein-coding potential (18). It is evident that lncRNAs have a wide range of biological functions, and their aberrant expression has been associated

with diverse pathological settings, including cancer, metabolic, and cardiovascular diseases (19–21). Emerging evidence has shown that lncRNAs may play a critical role in the pathogenesis of kidney diseases (22), and functional lncRNAs regulating renal inflammation and mitochondrial bioenergetics have been recently identified (23, 24). However, most of these studies were conducted using mouse lncRNAs. There are a limited number of studies on the functions of lncRNAs in the human kidney. Unlike other noncoding RNAs such as microRNAs and small nucleolar RNAs, which can exhibit high degrees of conservation across diverse species, lncRNAs often lack strong conservation (25, 26). Furthermore, the biological roles of lncRNAs in regulating human TIF remain elusive, and more detailed studies are needed to unravel the molecular functions of lncRNAs in this setting.

Here, we investigated the potential role of lncRNAs involved in the progression of renal fibrosis and their underlying mechanisms. We identified a kidney-enriched TGF- β /Smad3-interacting lncRNA, which we called *lnc-TSI*, that inhibited renal fibrogenesis through negative regulation of the TGF- β /Smad pathway. This discovery adds to our understanding of the complex regulation of TGF- β /Smad signaling and provides a potential new therapeutic target for renal fibrosis.

RESULTS

lnc-TSI is expressed in human TECs and is regulated by TGF- β 1 via a SMAD3-dependent mechanism

TGF- β 1/Smad signaling plays a critical role in the pathogenesis of TIF (2, 7, 8). To identify lncRNAs that are potentially involved in the TGF- β /Smad pathway, we first searched for lncRNA expression in TGF- β 1-stimulated human TECs (HK2 and HKC8 cells) using microarrays. We found that nine lncRNAs were up-regulated and two were down-regulated by more than fivefold (table S1). Through microarray profiling (Fig. 1A), we identified *lnc-TSI* as the most up-regulated lncRNA upon TGF- β 1 stimulation. *lnc-TSI* was located at human chromosome 21 and was poorly conserved across species,

¹Division of Nephrology, Nanfang Hospital, Southern Medical University, State Key Laboratory of Organ Failure Research, National Clinical Research Center of Kidney Disease, Guangzhou 510515, China. ²Guangdong Provincial Key Laboratory of Malignant Tumor Epigenetics and Gene Regulation, Sun Yat-sen Memorial Hospital, Sun Yat-sen University, Guangzhou 510120, China.

*These authors contributed equally to this work.

†Corresponding author. Email: fhouguangzhou@163.com

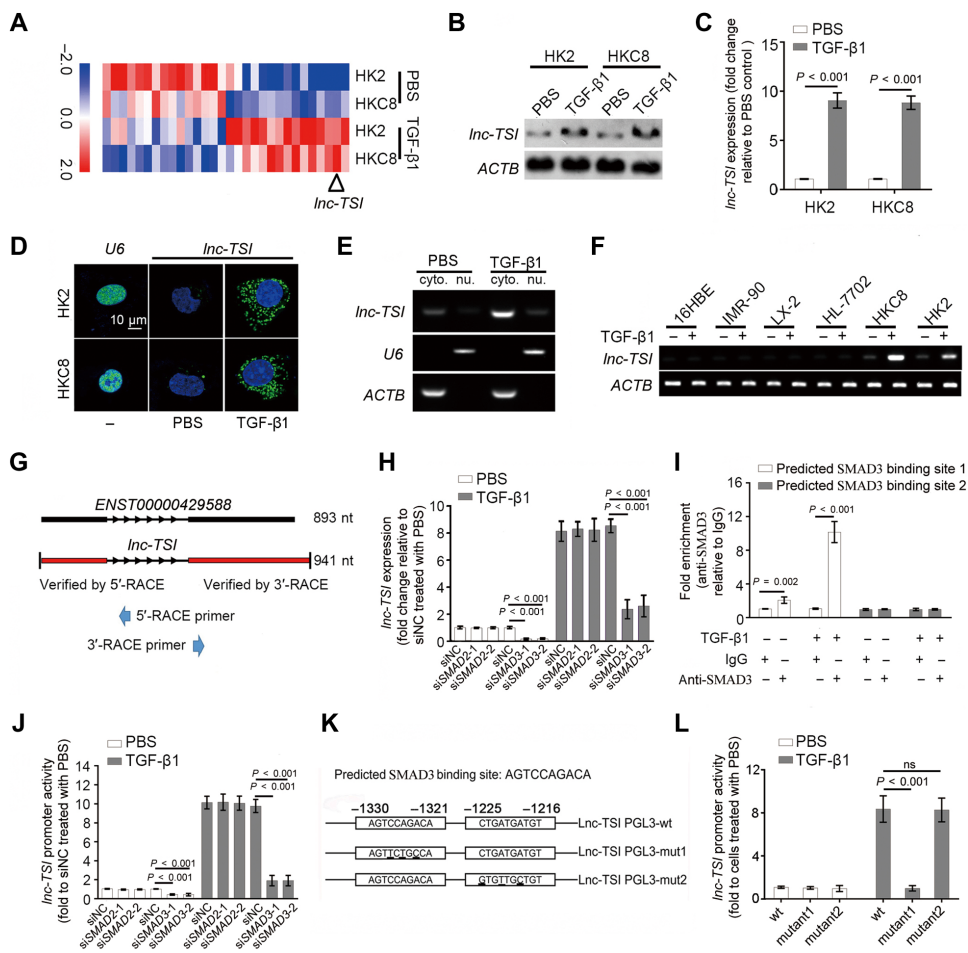


Fig. 1. *Inc-TSI* is expressed in human TECs and regulated by TGF- β 1 via a SMAD3-dependent mechanism. (A) Heat map of expression changes greater than twofold of lncRNAs in TECs cultured with TGF- β 1 for 24 hours. (B) Northern blot for *Inc-TSI* in HK2 and HKC8 cells treated with TGF- β 1 (10 ng/ml) for 24 hours. (C) Expression of *Inc-TSI* assayed by qRT-PCR. (D) Confocal FISH images showing cytoplasmic localization of *Inc-TSI* in HK2 and HKC8 cells. U6 small nuclear RNA was used as control. (E) RT-PCR showing *Inc-TSI* expression in the cytoplasm (cyto.) and nucleus (nu.) fractions of HK2 treated with TGF- β 1 (10 ng/ml, 24 hours). (F) RT-PCR showing low expression of *Inc-TSI*, with or without TGF- β stimulation, in human bronchial epithelial cells (16HBE), human lung fibroblast cells (IMR-90), human hepatic stellate cells (LX-2), and human hepatocyte cells (HL-7702) as compared to human TECs (HKC8 and HK2). (G) Full length of *Inc-TSI* (ENST00000429588) predicted in the UCSC Genome Browser and measured *Inc-TSI* acquired by 5' and 3' RACE. (H) Knocking down *SMAD3* decreased the expression of *Inc-TSI* assayed by qRT-PCR in HK2 cells with or without TGF- β 1 stimulation. (I) ChIP assay showing that SMAD3 bound to SMAD3-binding site 1 in the *Inc-TSI* promoter under TGF- β 1 stimulation (10 ng/ml, 2 hours). (J) Knocking down *SMAD3* decreased the transcription of *Inc-TSI*, as detected by luciferase reporter assays. (K) Mutation strategies for the *Inc-TSI* promoter. The underlined nucleotides indicate the mutated nucleotides. (L) Mutation of SMAD3-binding site 1 reduced *Inc-TSI* transcription in luciferase reporter assays. As a control, an equivalent amount of phosphate-buffered saline (PBS) was added to the culture medium. Data are expressed as means \pm SD of three independent experiments in (C), (H) to (J), and (L). Student's *t* test and one-way analysis of variance (ANOVA) were used for comparison between two groups and multiple groups, respectively. ns, not significant.

as a clear orthologous counterpart could not be identified in the mouse genome via BLAST (Basic Local Alignment Search Tool). Northern blots and quantitative reverse transcription polymerase chain reaction (qRT-PCR) confirmed that *Inc-TSI* was constitutively expressed in human TECs and was up-regulated after TGF- β 1 stimulation (Fig. 1, B and C, and fig. S1A). The expression of *Inc-TSI* in response to TGF- β 1 was dose- and time-dependent (fig. S1, B and C). Fluorescence in situ hybridization (FISH) demonstrated

that *Inc-TSI* localized primarily to the cytoplasm of TECs (Fig. 1D), which we verified by RT-PCR of the nuclear and cytoplasmic fractionations (Fig. 1E).

To further determine the tissue specificity of *Inc-TSI*, we examined the expression of *Inc-TSI* in cultured cells of other epithelial parenchymal tissues in the presence or absence of TGF- β 1. Expression of *Inc-TSI* was low in human liver and lung cells, either with or without TGF- β 1, compared to that in TECs (Fig. 1F). *Inc-TSI* expression, as determined by in situ hybridization and RT-PCR, was up-regulated in human fibrotic kidney but not in fibrotic liver or lung (fig. S1, D and E). In kidney, *Inc-TSI* was expressed predominantly in the cytoplasm of proximal TECs and was up-regulated upon TGF- β 1 stimulation in vitro (fig. S1, F and G).

In the UCSC (University of California Santa Cruz) Genome Browser (27), we found *Inc-TSI* labeled as AP000695.6 or ENST00000429588.1. To determine the exact sequence of *Inc-TSI*, we performed 5' and 3' rapid amplification of complementary DNA ends (RACE) and found that *Inc-TSI* was a 941-nt lncRNA (Fig. 1G, fig. S1H, and data file S1). *Inc-TSI* did not have a representative protein-coding open reading frame (ORF) longer than 300 nt according to ORF Finder (28). As *Inc-TSI* expression was up-regulated by TGF- β 1, we investigated the role of SMAD2 and SMAD3, key factors in TGF- β 1 pathway, in *Inc-TSI* transcription. The expression of *Inc-TSI* decreased when SMAD3 was silenced with small interfering RNAs (siRNAs; Fig. 1H) and SMAD2 knockdown did not affect the expression of *Inc-TSI* (Fig. 1H and fig. S1, J and K), suggesting that the transcription of *Inc-TSI* was SMAD3-dependent.

Next, we performed chromatin immunoprecipitation (ChIP) analysis with an anti-SMAD3 antibody to determine whether SMAD3 could bind to the *Inc-TSI* promoter. According to JASPAR, a database of transcription factor binding profiles (29), there are two predicted potential SMAD3-binding sites in the promoter region of *Inc-TSI* [-1321 to -1330 base pairs (bp) and -1766 to -1776 bp in human genome build hg38]. Our ChIP analysis demonstrated the interaction between SMAD3 and promoter region of *Inc-TSI* (-1321 to -1330 bp), indicating that *Inc-TSI* is a transcriptional target of SMAD3 (Fig. 1I). To confirm, we cloned the promoter region between -1 and -2000 bp into a pGL3-enhancer vector. A luciferase reporter assay demonstrated

that silencing SMAD3, but not SMAD2, reduced *lnc-TSI* promoter activity (Fig. 1J). We further constructed a series of pGL3 reporter plasmids containing a mutant or wild-type region between -1216 to -1225 bp and -1321 to -1330 bp (Fig. 1K). Mutation of the SMAD3-binding site (-1321 to -1330 bp) reduced luciferase activity, whereas mutation of the promoter sequence downstream of the SMAD3-binding site (-1216 to -1225 bp) did not influence the transcriptional activity (Fig. 1L). These data suggest that Smad3 binds with the promoter of *lnc-TSI* and up-regulates the expression of *lnc-TSI*.

***lnc-TSI* inhibits TGF- β 1-induced SMAD3 phosphorylation in human TECs**

To determine the role of *lnc-TSI* in regulating TGF- β /Smad signaling, we knocked down *lnc-TSI* in HK2 or HKC8 cells by siRNA or lentivirus carrying *lnc-TSI* short hairpin RNAs (shRNAs). Real-time PCR showed that both methods efficiently reduced *lnc-TSI* expression in HK2 or HKC8 cells in the presence or absence of TGF- β stimulation (fig. S2, A to C).

We ectopically expressed *lnc-TSI* in human TECs by transfecting the cells with pcDNA3.1 vector carrying the full-length sequence of *lnc-TSI* (fig. S2, D and E). Knocking down *lnc-TSI* increased TGF- β 1-induced SMAD3 phosphorylation without affecting SMAD2 phosphorylation (Fig. 2A). Transcription of *SMAD3* and expression of SMAD4 and SMAD7 were not affected by either silencing or overexpressing *lnc-TSI* (fig. S2, F and G). Conversely, overexpression of *lnc-TSI* inhibited SMAD3, but not SMAD2, phosphorylation in HK2 cells (Fig. 2B).

Translocation of Smad complexes into nuclei is a crucial step of TGF- β signaling (11). We fractionated the nuclei and cytoplasm of HK2 cells to investigate Smad nuclear translocation. Upon TGF- β 1 stimulation, knocking down *lnc-TSI* enhanced SMAD3, SMAD2, and SMAD4 nuclear translocation (Fig. 2C and fig. S2H), whereas overexpression of *lnc-TSI* inhibited the translocation of these Smads into nuclei (Fig. 2D and fig. S2I). Immunofluorescence staining confirmed that forced expression of *lnc-TSI* in HK2 cells abrogated TGF- β 1-induced SMAD3 nuclear translocation, and silencing *lnc-TSI* notably enhanced the translocation (Fig. 2E). Furthermore, overexpression of *lnc-TSI* substantially decreased TGF- β 1-induced expression of SMAD3 target genes, including *SNAIL1*, *COL1A1*, and α SMA (Fig. 2F), whereas knocking down *lnc-TSI* enhanced their expression (Fig. 2G). We validated these effects of *lnc-TSI* on the phosphorylation of SMAD3 and downstream responses using CRISPR-Cas9 (fig. S3). These data suggest that *lnc-TSI* negatively regulates the TGF- β /Smad3 pathway by specifically inhibiting the phosphorylation and subsequent nuclear translocation of SMAD3.

***lnc-TSI* binds to the MH2 domain of SMAD3 and blocks the interaction between T β RI and SMAD3**

We next explored the molecular mechanism underlying *lnc-TSI*-induced inhibition of SMAD3 phosphorylation. To identify potential *lnc-TSI*-interacting proteins, we performed RNA pull-down assays in vitro with biotinylated *lnc-TSI*, followed by mass spectrometry. In total, we identified seven proteins that associated with *lnc-TSI* (table S2). Among them, three (SMAD3, α -tubulin, and β -tubulin) were confirmed to bind *lnc-TSI* by RNA pull-down (Fig. 3, A to C) and RNA immunoprecipitation (RIP; fig. S4, A and B). Other TGF- β signaling-related proteins, such as SARA, T β RI, SMAD2, SMAD4, and SMAD7, were not bound with *lnc-TSI* (Fig. 3C). Consistent with this,

a RIP assay showed that immunoprecipitation of SMAD3 or FLAG-tagged SMAD3, but not other TGF- β signaling-related proteins, retrieved *lnc-TSI* upon TGF- β 1 stimulation (fig. S4B). In addition, *lnc-TSI* FISH followed by immunofluorescence of SMAD3 demonstrated colocalization of *lnc-TSI* with SMAD3 in the cytoplasm of HK2 cells treated with TGF- β 1 (Fig. 3D).

Although α - and β -tubulin can bind with *lnc-TSI*, knocking down these proteins did not affect the TGF- β 1-induced SMAD3 phosphorylation (fig. S4, C and D), suggesting that α - and β -tubulin did not affect the regulatory effect of *lnc-TSI*. Knocking down or overexpressing *lnc-TSI* did not affect the mRNA expression of the genes neighboring *lnc-TSI* (fig. S4, E and F).

To determine the nucleotide sequence of *lnc-TSI* that binds SMAD3, we prepared a series of *lnc-TSI* deletion mutants. As shown in Fig. 3E, mutants containing nt 301 to 450 of *lnc-TSI* exhibited binding with SMAD3 comparable to that of the full-length *lnc-TSI*, suggesting that nt 301 to 450 of *lnc-TSI* are critical for the interaction of *lnc-TSI* with SMAD3. According to the Mfold (30) and RNAfold (31) packages, there are two stem-loop structures within nt 301 to 450 of *lnc-TSI*, termed stem-loop A (nt 310 to 333) and stem-loop B (nt 340 to 411; Fig. 3F). Mutation of either stem-loop A or stem-loop B completely abolished binding of *lnc-TSI* with SMAD3 (Fig. 3G), suggesting that stem-loops A and B were sites where *lnc-TSI* bound with SMAD3. To determine the precise binding sites of SMAD3 with *lnc-TSI*, we generated full-length or truncated SMAD3 constructs (Fig. 3H). RIP (Fig. 3I and fig. S4G) and RNA pull-down assays (Fig. 3J) demonstrated that *lnc-TSI* bound to the MH2 domain of SMAD3, a recognized binding domain of the cytoplasmic tail of T β RI (12).

Coimmunoprecipitation of SMAD3 or T β RI with T β RI-interacted proteins (SARA or SMAD2) demonstrated that knocking down *lnc-TSI* enhanced the interaction between SMAD3 and T β RI but did not change the interaction between SMAD3 and SARA or SMAD2 and T β RI (Fig. 3K and fig. S4H). Although overexpression of *lnc-TSI* hindered the interaction between T β RI and SMAD3 in a dose-dependent manner, it did not influence the interaction between SMAD3 and SARA, T β RI, or SMAD2 (Fig. 3L and fig. S4, I and J). Neither knocking down nor overexpressing *lnc-TSI* affected epidermal growth factor (EGF)-induced SMAD3 phosphorylation at Ser²⁰⁸ of the linker domain (fig. S4, K to M) (32).

Ectopic expression of human *lnc-TSI* in mouse TECs inhibits TGF- β /Smad signaling

As mouse proximal tubular epithelial cells (mTECs) do not express *lnc-TSI*, we therefore evaluated whether ectopic expression of human *lnc-TSI* in mTECs may affect TGF- β 1/Smad signaling in these cells. Human *lnc-TSI* was efficiently transfected into mTECs (Fig. 4, A to C). Transfection of *lnc-TSI* into mTECs suppressed TGF- β 1-induced phosphorylation of Smad3 without affecting Smad2 phosphorylation (Fig. 4D) and attenuated the expression of profibrotic genes downstream of Smad3 at both mRNA and protein levels (Fig. 4, E and F).

The protein sequence of Smad3 is highly conserved and identical between human and mouse. An RNA pull-down assay indicated that *lnc-TSI* could bind to mouse Smad3 (Fig. 4G). A RIP assay confirmed that mouse Smad3 could retrieve human *lnc-TSI* transfected into mTECs (Fig. 4H). Transfection of *lnc-TSI* in mTECs inhibited the interaction of Smad3 with T β RI in a dose-dependent manner but did not affect the interaction of Sara or Smad2 with T β RI (Fig. 4I).

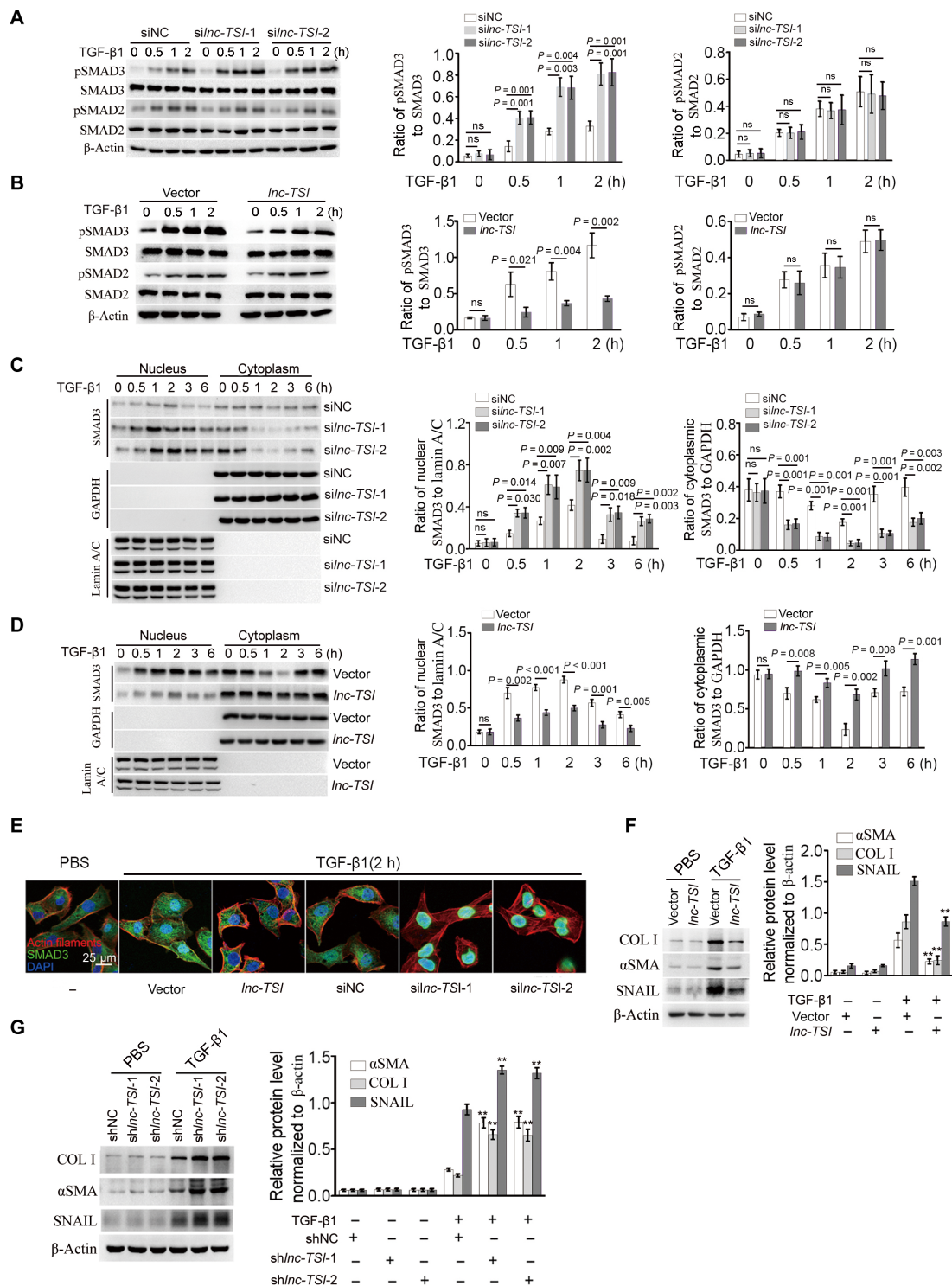


Fig. 2. *Inc-TSI* inhibited TGF-β1-induced SMAD3 phosphorylation in human TECs. (A) Silencing *Inc-TSI* upon transfection with siRNAs promoted SMAD3, but not SMAD2, phosphorylation in TGF-β1-treated HK2 cells. **(B)** Overexpression of *Inc-TSI* upon transfection with pcDNA3.1-*Inc-TSI* inhibited SMAD3, but not SMAD2, phosphorylation in HK2 cells incubated with TGF-β1. **(C)** Silencing *Inc-TSI* by siRNA promoted the nuclear translocation of SMAD3 in HK2 cells stimulated with TGF-β1 (10 ng/ml). GAPDH, glyceraldehyde-3-phosphate dehydrogenase. **(D)** Overexpression of *Inc-TSI* by pcDNA3.1-*Inc-TSI* inhibited SMAD3 nuclear translocation. **(E)** A representative photo of SMAD3 nuclear translocation, assayed by immunofluorescence confocal microscopy, in HK2 cells with *Inc-TSI* silenced or overexpressed. DAPI, 4',6-diamidino-2-phenylindole. **(F)** Overexpression of *Inc-TSI* decreased the expression of SMAD3 downstream genes in TGF-β1-treated HK2 cells. **(G)** Transfecting HK2 cells with *Inc-TSI* shRNAs increased SMAD3 downstream genes under TGF-β1 stimulation. Data are expressed as means ± SD of three independent experiments. Student's *t* test and one-way ANOVAs were used for comparison between two groups and multiple groups, respectively. ***P* < 0.01.

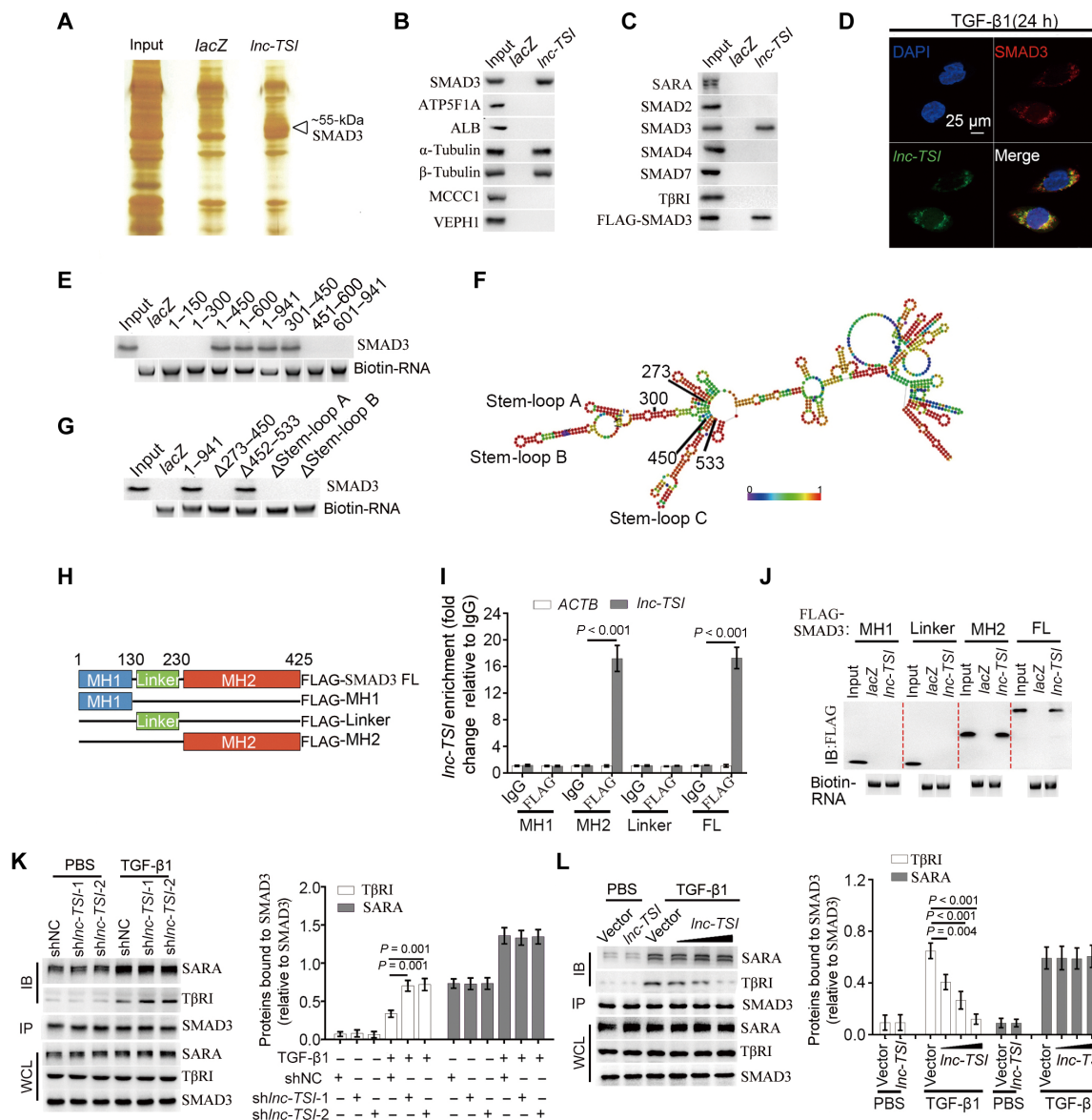


Fig. 3. *lnc-TSI* bound the MH2 domain of SMAD3 and blocked the interaction between TβRI and SMAD3. (A) Silver staining of proteins bound to *lnc-TSI* (right lane) or *lacZ* (middle lane). The RNA pull-down study was performed with HK2 cell lysates. A specific band (arrow) was identified as SMAD3 by mass spectrometry. (B) SMAD3, α-tubulin, and β-tubulin bound with *lnc-TSI* confirmed by Western blot after RNA pull-down. (C) *lnc-TSI* bound to endogenous and exogenous SMAD3 in HK2 cell lysates as shown by Western blotting after RNA pull-down. (D) Confocal images showing the colocalization of *lnc-TSI* and SMAD3 in HK2 cells treated with TGF-β1 for 24 hours. (E) RNA pull-down showing the interaction of sequentially deleted *lnc-TSI* mutants with SMAD3 in vitro. (F) *lnc-TSI* is predicted to have two stable stem-loop structures, stem-loop A (nt 310 to 333) and stem-loop B (nt 340 to 411). (G) RNA pull-down indicated that deletion mutations of stem-loop A and B (nt 273 to 450) abolished the binding ability of *lnc-TSI* to SMAD3. (H) To test the binding site of SMAD3 with *lnc-TSI*, deletion mutants of SMAD3 fragments were labeled by FLAG. (I) *lnc-TSI* bound with the MH2 domain of SMAD3 as shown by RIP followed by qRT-PCR. (J) Interaction of *lnc-TSI* with SMAD3 truncated mutants in vitro as shown by Western blotting after RNA pull-down in HK2 cell lysates. (K) Cell lysates of HK2 cells expressing *lnc-TSI* shRNA or shNC were immunoprecipitated (IP) with anti-SMAD3 antibody followed by immunoblotting (IB). Knocking down *lnc-TSI* increased the interaction between SMAD3 and TβRI. WCL, whole-cell lysate. (L) Overexpression of *lnc-TSI* decreased the interaction of SMAD3 with TβRI. Data are expressed as means ± SD of three independent experiments. Student's *t* test and one-way ANOVAs were used to compare two groups and multiple groups, respectively.

Delivery of human *lnc-TSI* alleviates renal fibrosis in mouse UUO and ischemic reperfusion injury-induced TIF

We used unilateral ureteral obstruction (UUO) mice to further explore the role of *lnc-TSI* in the pathogenesis of TIF in vivo. Animals were treated via hydrodynamic-based injection of human *lnc-TSI* plasmid or vector 2 days before and after operation (Fig. 5A). Northern

blots of kidney homogenates (Fig. 5B) and in situ hybridization in renal tissue (Fig. 5C) demonstrated the efficacy of delivering human *lnc-TSI* into mouse kidneys. In situ hybridization of *lnc-TSI* in mouse kidneys showed that *lnc-TSI* was mainly expressed in cortical tubule cells, with a transfection rate of about 50% (and rare expression observed in liver or spleen) (fig. S5).

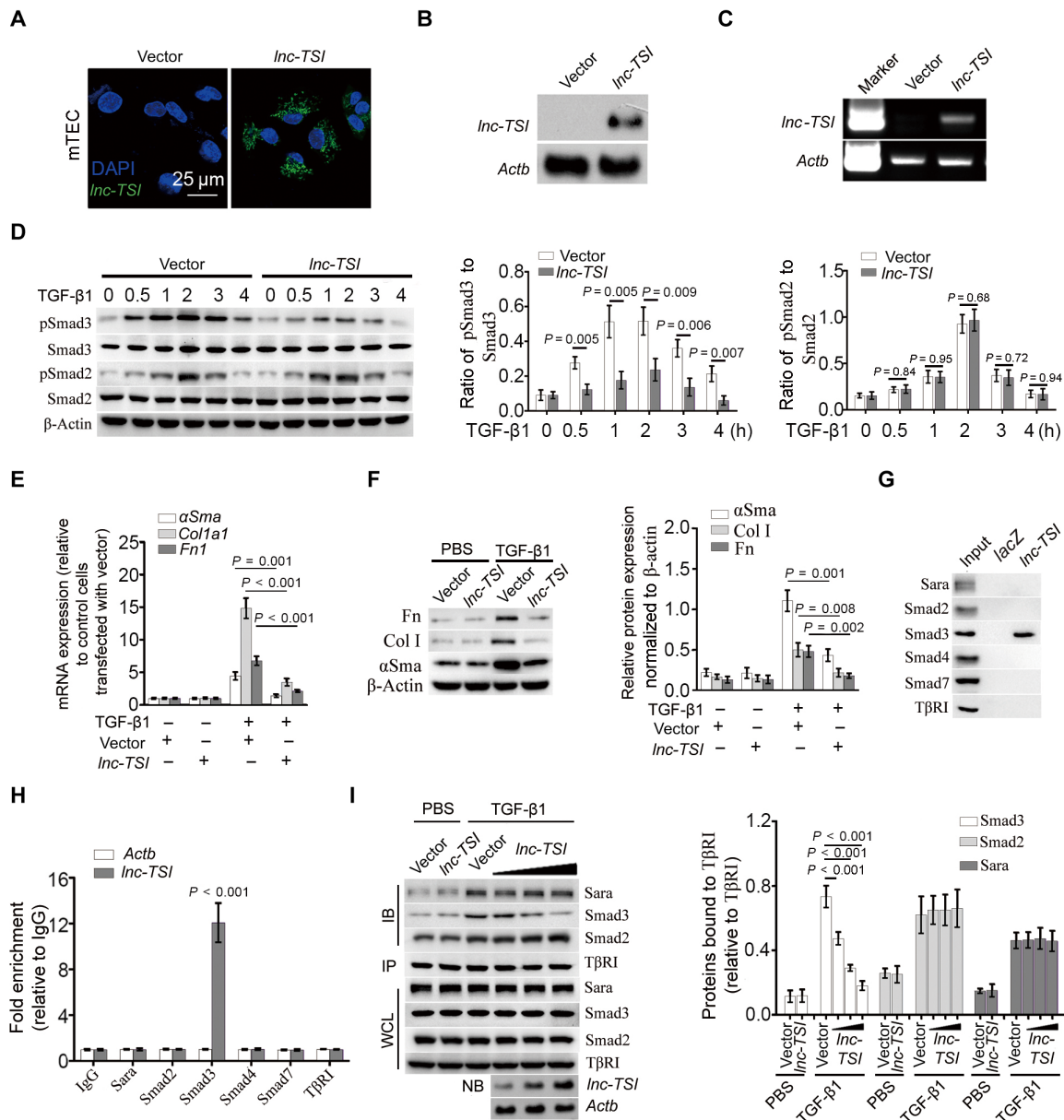


Fig. 4. Ectopic expression of human *Inc-TSI* in mouse TECs inhibited TGF- β /Smad signaling. (A) Confocal FISH images showing cytoplasmic localization of human *Inc-TSI* in mTECs. (B) Northern blotting showing expression of *Inc-TSI* in mTECs transfected with pcDNA3.1-*Inc-TSI*. (C) RT-PCR confirmed the presence of *Inc-TSI* in mTECs transfected with pcDNA3.1-*Inc-TSI*. (D) Forced expression of *Inc-TSI* inhibited Smad3 phosphorylation in mTECs treated with TGF- β 1 (10 ng/ml). (E and F) Transfection of *Inc-TSI* reduced the expression of Smad3 downstream genes at both mRNA (E) and protein (F) levels. (G) RNA pull-down followed by Western blotting confirmed the binding of human *Inc-TSI* to mouse Smad3 in mTECs transfected with pcDNA3.1-*Inc-TSI*. (H) RIP followed by qRT-PCR demonstrated the binding of human *Inc-TSI* to mouse Smad3 in mTECs transfected with pcDNA3.1-*Inc-TSI*. (I) Cell lysates from mTECs were immunoprecipitated with anti-T β R1 antibody, followed by immunoblotting using antibodies against T β R1, Sara, Smad2, and Smad3. NB, Northern blotting. Forced expression of human *Inc-TSI* in mTECs transfected with pcDNA3.1-*Inc-TSI* decreased the interaction between mouse T β R1 and Smad3 in a dose-dependent manner. Data are expressed as means \pm SD of three independent experiments. Student's *t* test and one-way ANOVAs were used to compare two groups and multiple groups, respectively.

Ectopic expression of *Inc-TSI* substantially alleviated TIF in UUO mice, as shown by **Masson staining** and TIF index in the kidney (Fig. 5, D and E). Mechanistically, the RIP analysis showed that Smad3 was coprecipitated with *Inc-TSI* in kidney homogenates from mice injected with *Inc-TSI* plasmid (Fig. 5F). Moreover, the delivery of *Inc-TSI* inhibited Smad3 activation in the kidney and down-regulated the expression of its target profibrotic genes, in-

cluding *alphaSma*, *Col1a1*, and *Fn1*, at both mRNA and protein levels (Fig. 5, G to J). To confirm the anti-fibrotic effect of *Inc-TSI*, we also treated UUO mice with **adeno-associated virus (AAV)-carrying human *Inc-TSI* 7 days before operation**. The infection rate of tubular cells in the cortex by AAV was above 50%, and we observed improvement of TIF index in animals infected with AAV-carrying human *Inc-TSI* (fig. S5, G to L).

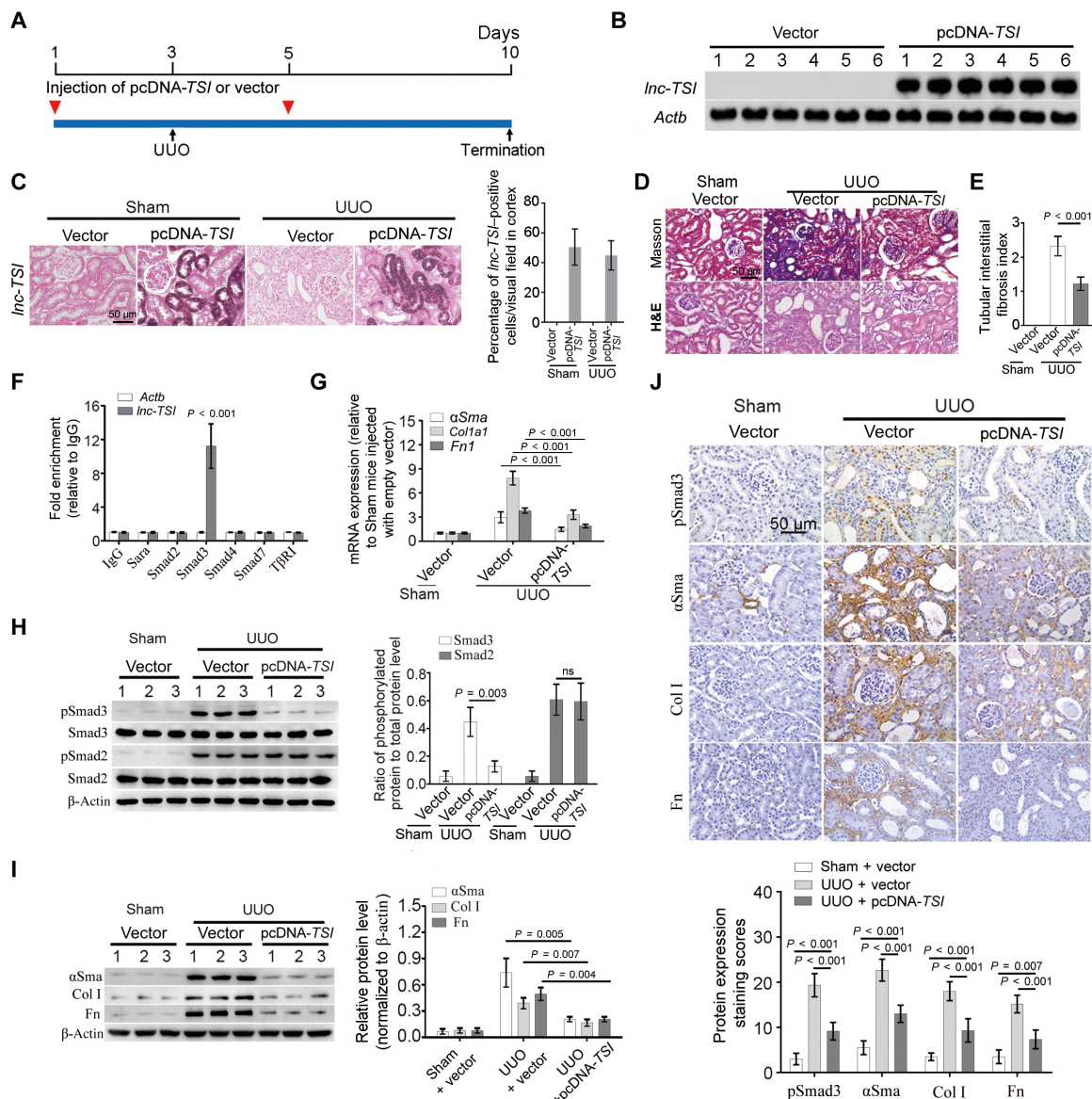


Fig. 5. Delivery of human *Inc-TSI* alleviated renal fibrosis in a mouse UUO model. (A) Mice were treated by intravenous injection of either pcDNA3.1-*Inc-TSI* (pcDNA-TSI) or pcDNA3.1 empty vector (vector) 2 days before and after UUO surgery. Animals were euthanized 7 days after UUO. (B) Northern blotting showing *Inc-TSI* expression in the kidney homogenates from UUO mice injected with pcDNA-TSI. (C) Representative images of in situ hybridization of *Inc-TSI* expression in kidneys from mice injected with pcDNA-TSI (left) and the percentage of *Inc-TSI*-positive tubular cells in renal cortex (right). (D) Masson's trichrome and hematoxylin and eosin (H&E) staining of renal sections from mice injected with pcDNA-TSI. (E) Forced expression of human *Inc-TSI* in UUO mice reduced renal tubular interstitial fibrosis indexes compared to mice treated with empty vector. (F) RIP followed by qRT-PCR showing binding of human *Inc-TSI* with mouse Smad3 in kidney homogenates from mice injected with pcDNA-TSI. (G) Quantification by RT-PCR showed that exogenous *Inc-TSI* decreased the mRNA expression of *alphaSma*, *Col1a1*, and *Fn1* in kidney homogenates. (H) Delivery of human *Inc-TSI* reduced expression of pSmad3 but did not affect expression of pSmad2 in UUO kidneys. (I) Forced expression of human *Inc-TSI* down-regulated expression of α SMA, collagen I (Col I), and fibronectin (Fn) in UUO kidney. (J) Representative images of immunohistochemical staining of pSmad3, α SMA, collagen I, and fibronectin in Sham and UUO model treated with pcDNA-TSI or empty vector (up) with data analysis (down). Data are expressed as means \pm SD. Student's *t* test and one-way ANOVAs were used for the comparison of two groups and multiple groups, respectively ($n = 6$ for each group).

To highlight the therapeutic potential of TSI, we injected mice three times with *Inc-TSI* plasmid at different time points (days 3, 5, and 7) after UUO surgery. Treatment with AAV delivery of *Inc-TSI* ameliorated the established TIF in this model (Fig. 6, A to F). Similarly, in a unilateral ischemic reperfusion injury (IRI)-induced renal fibrosis model, treatment with hydrodynamic-based injection of pcDNA3.1-*Inc-TSI* ameliorated IRI-induced renal fibrosis and improved renal function post-ischemia (Fig. 6, G to M).

Intrarenal *Inc-TSI* is up-regulated and negatively correlates with renal fibrosis in patients with fibrotic kidney disease

To evaluate the role of *Inc-TSI* in the pathogenesis of human TIF, we conducted a cross-sectional analysis for the association of *Inc-TSI* expression and TIF in a cohort of 58 patients with biopsy-proven immunoglobulin A (IgA) nephropathy (IgAN), a chronic kidney disease with the potential to progress to renal fibrosis. Characteristics of patients at time of diagnosis (initial biopsy) were shown in

Fig. 6. Delivery of human *Inc-TSI* ameliorated renal fibrosis in established UUO and IRI-induced TIF models. (A) Mice were treated with intravenous injection of either pcDNA3.1-*Inc-TSI* (pcDNA-*TSI*) or pcDNA3.1 empty vector (Vector) at third, fifth, and seventh days after processing UUO. Animals were euthanized 10 days after UUO. **(B)** Northern blotting showing *Inc-TSI* expression in kidney homogenates from UUO mice injected with pcDNA-*TSI*. **(C)** Representative images of in situ hybridization of *Inc-TSI* expression in mice injected with pcDNA-*TSI* (left) and the percentage of *Inc-TSI*-positive tubular cells in renal cortex (right). **(D)** Representative images of Masson's trichrome and immunohistochemical staining of pSmad3 in mice treated with pcDNA-*TSI* or empty vector. **(E and F)** Delivery of human pcDNA-*TSI* in UUO mice reduced renal tubular interstitial fibrosis indexes (E) and pSmad3 expression (staining scores) (F) compared to mice treated with empty vector. **(G)** Mice were treated by either pcDNA-*TSI* or empty vector after establishing IRI. **(H)** Northern blotting showing *Inc-TSI* expression in kidney homogenates from IRI mice injected with pcDNA-*TSI*. **(I)** Representative images of *Inc-TSI* in situ hybridization in mice injected with pcDNA-*TSI* (left) and the percentage of *Inc-TSI*-positive cells in the renal cortex (right). **(J)** Representative images of Masson's trichrome and immunohistochemical staining of pSmad3 in the IRI model treated with pcDNA-*TSI* or empty vector. **(K and L)** Delivery of human *Inc-TSI* in IRI mice reduced renal tubular interstitial fibrosis indexes (K) and pSmad3 staining scores (L) compared to mice treated with empty vector. **(M)** Delivery of human *Inc-TSI* in IRI mice reduced the levels of serum creatinine at 11th day after IRI compared with the IRI mice injected with vector. Data are expressed as means ± SD. Student's *t* test and one-way ANOVAs were used for comparison of two groups and multiple groups, respectively (*n* = 6 for each group).

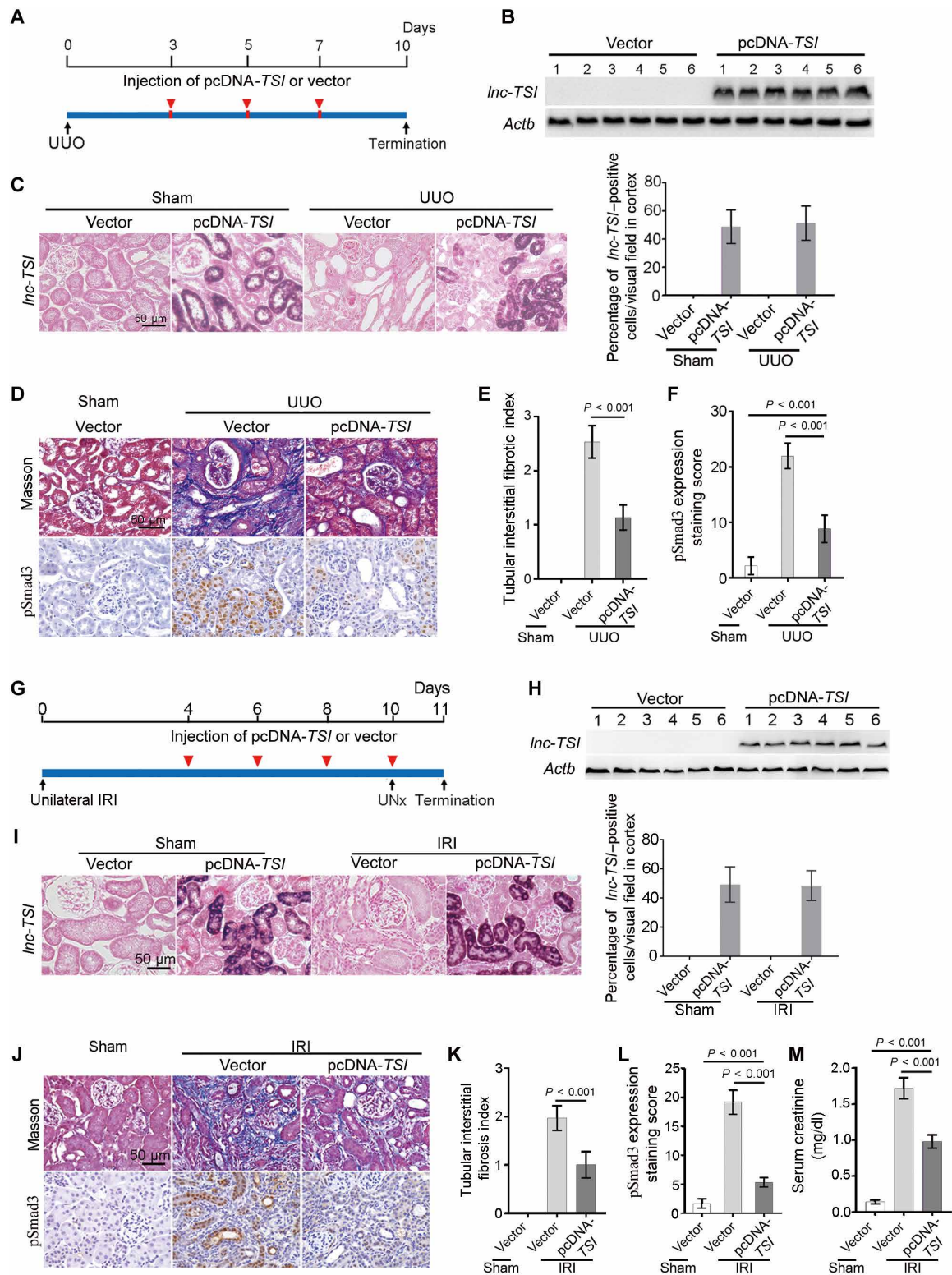


table S3. Among these patients, 72% had renal tubulointerstitial injury at initial renal biopsy with Oxford MEST-T grade ≥ 1 and a median TIF index of 0.7. In situ hybridization of *lnc-TSI* (Fig. 7A) and RT-PCR (fig. S1E) showed that normal human kidney (tissue adjacent to renal carcinoma) constitutively expressed *lnc-TSI* in TECs. Expression of *lnc-TSI* was obviously up-regulated in renal biopsy samples from patients with IgAN. We found that SMAD3 was expressed in almost all tubulars, whereas pSMAD3 expression was found only in some of the TECs. Higher expression of *lnc-TSI* was associated with weaker pSMAD3 expression (Fig. 7B). **Partial correlation analysis** showed a significant negative association between renal *lnc-TSI* expression and TIF index after adjusting the confounders such as mean arterial blood pressure and urinary protein excretion (Fig. 7C). *lnc-TSI* expression levels in kidney were also negatively correlated with pSMAD3 expression in a partial correlation analysis (Fig. 7D).

For the longitudinal study, 32 patients with IgAN were followed up and received repeat renal biopsies at a mean duration of 48 months. All of these patients were treated with **renin-angiotensin system inhibitors**, and 23 (72%) received **prednisone** for a length of time. The characteristics of these patients are presented in table S4. The median renal *lnc-TSI* expression score at initial biopsy was 15. After follow-up at a mean of 48 months, patients with *lnc-TSI* expression less than the median at the initial biopsy had a greater increase in their TIF index and Oxford MEST-T grade at the repeat biopsy (Fig. 7, E and F) and more pronounced decline in renal function represented by estimated glomerular filtration rate (eGFR) compared to those with baseline *lnc-TSI* expression greater than or equal to the median (Fig. 7G).

To confirm the effect of *lnc-TSI* in human TIF, we detected the expression of *lnc-TSI* in a cohort of patients with chronic tubulointerstitial disease induced by **aristolochic acid or uric acid nephropathy**, which are well known non-immune-associated kidney diseases. The expression pattern of *lnc-TSI* in this cohort was comparable to that in IgAN patients (fig. S6).

DISCUSSION

In this study, we identified an lncRNA that functioned as a negative regulator of the TGF- β 1/Smad3 pathway. *lnc-TSI* reduced renal fibrogenesis in humanized mice and may serve as a potential therapeutic target.

Phosphorylation of Smad3 by T β RI has been documented as a key initial

event in the activation of the TGF- β /Smad pathway. Although several proteins and molecules have been reported to regulate the interaction between T β RI and Smads (33–35), there remains a large gap in understanding the mechanism underlying the key event. We provided several lines of evidence demonstrating that *lnc-TSI* is a regulator of the interaction between T β RI and Smad3. The effect of *lnc-TSI* was independent of Smad7, a known classical inhibitor of TGF- β /Smad signaling (36–38). In our study, there was no interaction between *lnc-TSI* and Smad7 in RNA pull-down or RIP assays, and neither knocking down nor overexpressing *lnc-TSI* affected the expression of Smad7. Although both *lnc-TSI* and Smad7 act by specifically inhibiting the phosphorylation of Smad3, the

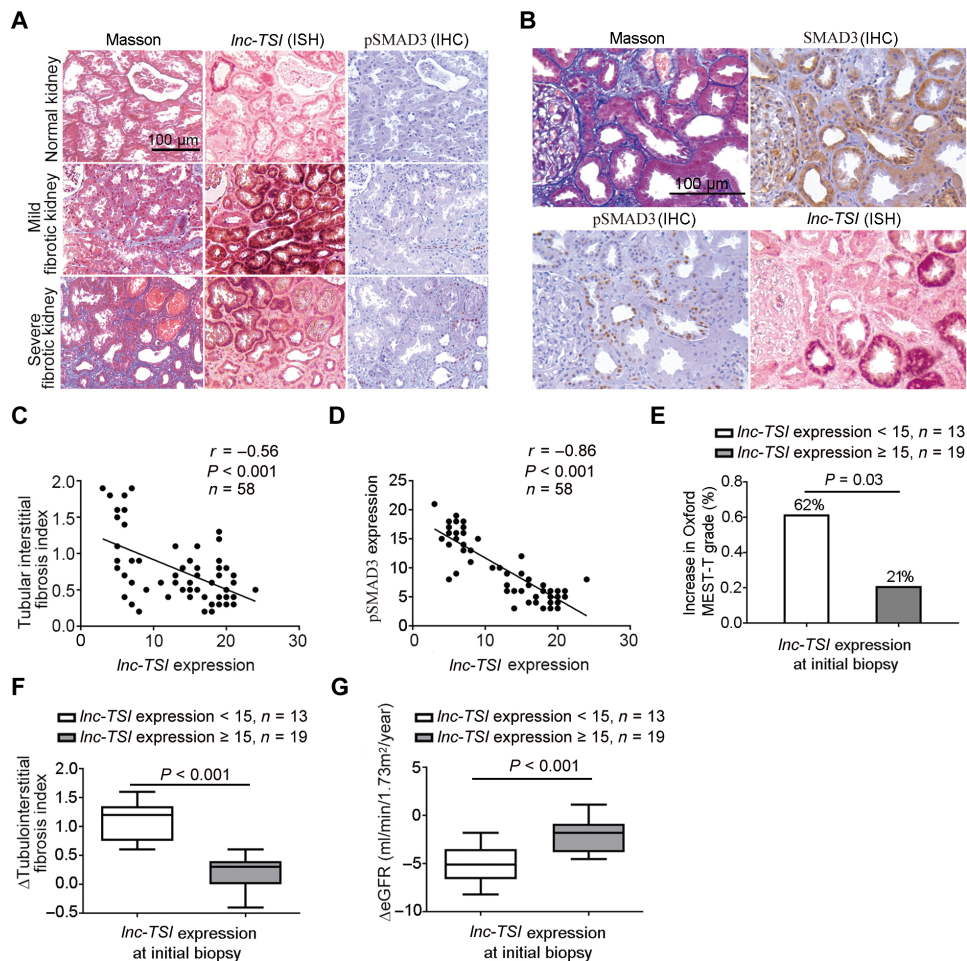


Fig. 7. Intrarenal *lnc-TSI* was up-regulated and negatively correlated with renal fibrosis in patients with IgAN.

(A) Representative photos of renal sections from normal kidney and biopsy samples from patients with IgAN. Expression of *lnc-TSI* was up-regulated in kidneys from patients with IgAN. IHC, immunohistochemistry. (B) Representative serial sections of renal biopsy from patients with IgAN. (C) The expression of renal *lnc-TSI* at initial biopsy negatively correlated with the tubular interstitial fibrosis index in a partial correlation analysis after adjusting for mean arterial blood pressure and urinary protein excretion. (D) The expression of renal *lnc-TSI* negatively correlated with pSMAD3 expression in a partial correlation analysis after adjusting for mean arterial blood pressure and urinary protein excretion. (E to G) Thirty-two patients with IgAN were followed up and received repeat renal biopsy at a mean duration of 48 months. Comparing to those with baseline renal *lnc-TSI* expression greater than or equal to the median, patients with *lnc-TSI* expression less than the median at the initial biopsy had a higher proportion showing an increase in Oxford MEST-T grade at the repeat biopsy. P values were calculated by the χ^2 test. (E) Those with lower expression of *lnc-TSI* at the initial biopsy also had a more pronounced increase in Δ TIF index (F) and a more pronounced decline in eGFR (G). Data in (F) and (G) are presented as box-and-whisker plots to show quartiles (boxes) and range (whiskers). P values were calculated by Student's t test.

mechanisms of blocking the access of Smads to T β RI are different. *lnc-TSI* blocked this interaction by binding with the MH2 domain of Smad3, whereas Smad7 is known to act either by forming a stable complex with activated T β RI or by causing degradation of T β RI (38, 39). Smad3 controlled *lnc-TSI* expression through binding with the promoter of *lnc-TSI* under TGF- β 1 stimulation, thereby up-regulating expression of *lnc-TSI* in TECs. Therefore, in conditions with increased TGF- β , such as inflammatory kidney disease, *lnc-TSI* may function as a negative regulator of the TGF- β 1/Smad pathway. The feedback loop formed among TGF- β 1, Smad3, and *lnc-TSI* is shown in fig. S7.

We found that *lnc-TSI* may play an important role in the pathogenesis of TIF. It is well accepted that TGF- β 1/Smad3 is a key pathway in the pathogenesis of TIF in both human and experimental animal kidney diseases (40). Delivery of human *lnc-TSI* to mouse TECs decreased TGF- β 1-induced expression of profibrotic genes and improved renal fibrosis in the well-established UUU-induced chronic model of TIF (41) and IRI-induced TIF. As UUU is not meant to replicate human disease, we also tested *lnc-TSI* expression in patients with newly diagnosed IgAN, an inflammatory chronic kidney disease with the potential to progress to renal fibrosis. We found that expression of renal *lnc-TSI* was up-regulated in patients with IgAN. *lnc-TSI* expression in patient kidneys negatively correlated with the severity of TIF. We also detected the expression of *lnc-TSI* in an additional cohort of patients with chronic tubulointerstitial disease induced by aristolochic acid or uric acid nephropathy. Consistently, the expression pattern of *lnc-TSI* in this cohort was comparable with that seen in IgAN. In patients who had received repeat renal biopsies, lower expression of renal *lnc-TSI* at initial kidney biopsy was associated with a more pronounced decline in renal function and an increase in TIF at repeat renal biopsy 4 years later, suggesting that kidney-enriched *lnc-TSI* may regulate human renal fibrogenesis. An alternative possibility is that less *lnc-TSI* is produced as tubular atrophy, and this may be a good marker for renal fibrosis progression. We observed that *lnc-TSI* was only induced in the fibrotic kidney but not in liver or lung. The tissue-specific expression of lncRNAs has been reported in previous studies (42–44), with a recent study demonstrating that lncRNA *Wisper* controls cardiac fibrosis but not kidney fibrosis (45).

There are limitations to this study. We were not able to investigate the role of *lnc-TSI* in a tubule-specific *lnc-TSI* transgenic mouse, which may yield more convincing evidence. Moreover, we were not able to test the effect of *lnc-TSI* by knocking down the *lnc-TSI* in vivo as it is not expressed in mouse kidneys. In addition, the two mouse models we used do not directly reflect human diseases resulting in fibrogenesis in the kidney, and renal fibrosis in these models was only established over the course of several days before therapeutic treatment with *lnc-TSI*. Further studies will be needed to see whether *lnc-TSI* can be therapeutically targeted in humans.

In conclusion, our study identified a kidney-enriched lncRNA that function as an endogenous inhibitor of TGF- β 1/Smad3 pathway and regulated renal fibrogenesis. These findings provide novel information for understanding the mechanisms underlying TGF- β 1-mediated tissue fibrosis. Our work hints at the possibility of a new therapeutic target to halt the most damaging process in kidney diseases, although this remains to be confirmed by future studies.

MATERIALS AND METHODS

Study design

The aim of this study was to identify and evaluate whether tissue-specific lncRNAs were potentially suitable as therapeutic targets for TGF- β 1-mediated renal fibrosis. Using microarray analysis and RT-PCR, we identified the most up-regulated lncRNA in kidney upon TGF- β 1 stimulation, which we named *lnc-TSI*. Using in situ hybridization and RT-PCR, we evaluated the tissue specificity of *lnc-TSI* expression in various types of cells from epithelial parenchymal tissues, in the presence or absence of TGF- β 1, and in human fibrotic tissues (kidney, lung, and liver). Loss- and gain-of-function experiments were performed in human TECs to test the role of *lnc-TSI* in the TGF- β -mediated fibrotic response in vitro. The loss-of-function approach was validated using CRISPR-Cas9. To explore the molecular mechanism underlying *lnc-TSI*-induced inhibition of Smad3 phosphorylation, we performed RNA pull-down followed by mass spectrometry to identify *lnc-TSI*-associated proteins. RNA pull-down and RIP assays assessed the potential interaction of *lnc-TSI* with Smad3 or other Smads. Interaction between T β RI and Smad3 or other T β RI-associated proteins was determined by coimmunoprecipitation.

To examine the role of *lnc-TSI* in renal fibrosis in vivo, we chose UUU mice as a chronic model of TIF. Mice were randomly assigned to UUU and Sham operation groups. To test whether *lnc-TSI* may hold therapeutic potential in TIF, we conducted gain-of-function experiments by delivering human full-length *lnc-TSI* to UUU mice by hydrodynamic-based injection of an *lnc-TSI*-carrying plasmid or AAV9-carrying *lnc-TSI*. To test the effect of *lnc-TSI* on fibrosis, we performed hydrodynamic-based injection both 2 days before and 2 days after surgery, whereas AAV9 injection was conducted 7 days before surgery. To test a potential therapeutic effect of *lnc-TSI*, hydrodynamic-based injection of *lnc-TSI* was performed on days 3, 5, and 7 after UUU. Renal fibrosis was quantified by Masson's trichrome staining, and the extracellular matrix expression on kidney sections was scored by two pathologists in a blinded manner. All sample measurements were blinded.

To evaluate the role of *lnc-TSI* in the pathogenesis of human renal fibrosis, we conducted a cross-sectional analysis of the association between *lnc-TSI* expression and TIF in a cohort of 58 patients with biopsy-confirmed IgAN. Renal fibrosis in the biopsy samples was quantified by Masson's trichrome staining and scored by two pathologists in a blinded manner. Expression of *lnc-TSI* in the kidney biopsy samples was determined with in situ hybridization. Association between the levels of *lnc-TSI* expression and severity of TIF was analyzed with partial correlation analysis. For the longitudinal study, 32 patients with IgAN were followed up and received repeat renal biopsies at a mean of 48 months after initial biopsy. Patients were divided into two groups according to their median renal *lnc-TSI* expression at the initial biopsy (<15 and \geq 15). Changes in the renal fibrosis index, Oxford MEST-T grade, and eGFR at follow-up were compared between the two groups. siRNA oligos and primers used in this study (table S5), deletion mutants (table S6), and subject-level data for experiments with $n < 20$ (table S7) can be found in the Supplementary Materials.

Cell culture

The human TEC line HK2 [American Type Culture Collection (ATCC)], human mesangial cells (ScienCell), the human hepatocyte cell line HL-7702 (Shanghai Cell Bank of Chinese Academy of

Sciences), the human hepatic stellate cell line LX-2 (Merck Millipore), and the human lung fibroblast cell line IMR-90 (ATCC) were commercially available. The human bronchial epithelial cell line 16HBE was provided by the Guangzhou Institute of Respiratory Disease. HKC8 cells were a gift from L. Racusen (Johns Hopkins University), and immortalized mTECs were a gift from H.-Y. Lan (The Chinese University of Hong Kong).

Cells were grown in Dulbecco's modified Eagle's medium (DMEM)/Ham's F12 medium (Invitrogen) supplemented with 10% fetal bovine serum (Invitrogen). Human embryonic kidney (HEK) 293T cells (ATCC) were cultured in DMEM (Invitrogen) supplemented with 10% fetal bovine serum. These cells were cultured at 37°C in an atmosphere containing 5% CO₂. Human immortalized podocytes AB8/13, a gift from M. Saleem's laboratory, were cultured in RPMI 1640 medium supplemented with 10% fetal bovine serum (46). The cells were cultured at 33°C and differentiated at 37°C in an atmosphere containing 5% CO₂. In some experiments, cells were serum-starved overnight when they reached about 70% confluence and then incubated with indicated doses of recombinant TGF-β1 (R&D Systems) or EGF (PeproTech) for various times as indicated.

Animal models

UUO in mice

The UUO model was induced in male C57BL/6 mice (Guangdong Medical Animal Center, Guangzhou) when mice were at 6 to 8 weeks of age with body weight of 20 to 25 g, as previously described (47). Briefly, the left ureter of mice was ligated under anesthesia with intraperitoneal injection of sodium pentobarbital, and the UUO kidney was harvested for analysis at the indicated number of days after surgery. Sham-operated mice were used as controls.

IRI-induced TIF in mice

IRI-induced TIF was performed in male C57BL/6 mice (Guangdong Medical Animal Center) at 6 to 8 weeks of age with body weight of 20 to 25 g, as previously described (48), with minor modifications. Briefly, under general anesthesia by sodium pentobarbital, the left renal pedicle was clipped for 30 min using microaneurysm clamps (Fine Science Tools). After removal of the clamps, reperfusion of the kidneys was visually confirmed. The body temperature of the mice was maintained between 37° and 38°C by applying a temperature-controlled heating device. Ten days after the induction of IRI, the right kidney was surgically removed. Sham-operated mice were used as controls. All animal studies were approved by the Nanfang Hospital Animal Care Committee and were performed according to the institutional guidelines of Southern Medical University.

Human subjects

Cohort of patients with IgAN

A total of 58 patients with newly diagnosed, biopsy-confirmed primary IgAN [macroalbuminuria (urinary protein excretion > 0.3 g/day) and eGFR > 60 ml/min per 1.73 m², with or without hypertension] from Nanfang Hospital (Guangzhou, China) were included in our analysis. This cohort consisted of IgAN patients with low to moderate risk for disease progression at the time of diagnosis (49). We excluded patients with confounding diseases such as diabetes, liver disease, and infection, and those with nephrotic-range proteinuria (>3.5 g/day) at the time of diagnosis. No patients received any treatment before diagnostic renal biopsy. Clinical characteristics of the patients at initial biopsy are shown in table S3. Thirty-two

patients received repeat renal biopsy at a mean of 48 months of follow-up. The clinical characteristics of the patients at baseline are presented in table S4.

Cohort of patients with chronic tubulointerstitial disease

A total of 15 patients with biopsy-proven chronic tubulointerstitial disease (12 cases caused by aristolochic acid and 3 by uric acid nephropathy) were included in the study. Clinical characteristics of the patients are shown in table S3. The observational clinical study was approved by the Institutional Review Board of the National Clinical Research Center for Kidney Disease (Guangzhou, China). The human samples used in the study were approved by the Board. All of the study participants provided written informed consent.

Gene delivery in an animal model

Hydrodynamic-based injection of *lnc-TSI*

pcDNA3.1-human *lnc-TSI* or empty vector pcDNA3.1 (Invitrogen) was injected by intravenous injection, as previously described (50). Briefly, 10 μg of plasmid DNA was diluted in 1.6 ml of saline and injected via the tail vein within 10 s for each mouse.

AAV9 transduction of *lnc-TSI*

The full length of *lnc-TSI* was inserted into a pAV-MIR-GFP vector. After sequencing ensured accuracy of the vector, AAV (serotype 9) was packaged, purified, and titrated by Vigene Biosciences. AAV9 (1 × 10¹² copies) harboring either the *lnc-TSI* or the control sequence was injected through the left renal vein of mice (51). Briefly, under general anesthesia, the left kidney of the mouse was exposed. The renal vein was clamped by microaneurysm clamp, and AAV particles diluted in 100 μl of saline were injected into the vein using a 31-gauge needle. The clamp was removed 15 min after injection followed by suturing of the incision.

Statistical analysis

Continuous variables were expressed as means ± SD or median (interquartile range). Categorical variables were expressed as number (percentages). Data were tested for normality using Kolmogorov-Smirnov test, and variance homogeneity using Levene's test. For comparing normally distributed continuous variables, we used two-tailed Student's *t* test or one-way ANOVA with a Tukey's post hoc test. For comparing variables that were not normally distributed, we used the Mann-Whitney *U* test. The χ² test was used for the comparison of categorical variables. Partial correlations analyzed the associations between *lnc-TSI* expression and the TIF index or pSmad3 expression, adjusting for mean arterial blood pressure and urinary protein excretion. *P* < 0.05 was considered statistically significant.

SUPPLEMENTARY MATERIALS

www.sciencetranslationalmedicine.org/cgi/content/full/10/462/eaat2039/DC1
Materials and Methods

Fig. S1. Characterization of *lnc-TSI*.

Fig. S2. Changing *lnc-TSI* expression did not affect SMAD3 mRNA expression or SMAD4 or SMAD7 protein expression in human TECs.

Fig. S3. Knockout of *lnc-TSI* by CRISPR-Cas9 aggravated TGF-β1-induced SMAD3 phosphorylation in human TECs.

Fig. S4. Changing *lnc-TSI* expression did not affect neighboring gene expression or EGF-induced SMAD3 phosphorylation.

Fig. S5. AAV9-carrying human *lnc-TSI* alleviated UUO-induced TIF in mice.

Fig. S6. Intrarenal *lnc-TSI* was up-regulated and negatively correlated with TIF and pSMAD3 in human chronic tubulointerstitial disease.

Fig. S7. Schematic of the proposed feedback loop between *lnc-TSI* and SMAD3.

Table S1. Microarray profiles of lncRNAs up-regulated or down-regulated more than fivefold upon TGF- β 1 stimulation in HK2 and HKC8 cells.

Table S2. *Inc-TS1*-interacting proteins identified by mass spectrometry.

Table S3. Characteristics of patients with newly diagnosed IgAN or chronic tubulointerstitial disease.

Table S4. Characteristics of IgAN patients at the time of initial and repeat renal biopsies.

Table S5. siRNA oligos and primers.

Table S6. Sequences of stem-loops A, B, and C and deletion mutants of each stem-loop.

Table S7. Subject-level data for experiments with $n < 20$ (Excel file).

Data file S1. Sequence of *Inc-TS1*.

References (52–59)

REFERENCES AND NOTES

- A. A. Eddy, E. G. Neilson, Chronic kidney disease progression. *J. Am. Soc. Nephrol.* **17**, 2964–2966 (2006).
- E. P. Böttinger, M. Bitzer, TGF- β signaling in renal disease. *J. Am. Soc. Nephrol.* **13**, 2600–2610 (2002).
- A. A. Eddy, Overview of the cellular and molecular basis of kidney fibrosis. *Kidney Int. Suppl.* **4**, 2–8 (2014).
- Y. Liu, Cellular and molecular mechanisms of renal fibrosis. *Nat. Rev. Nephrol.* **7**, 684–696 (2011).
- P. Boor, T. Ostendorf, J. Floege, Renal fibrosis: Novel insights into mechanisms and therapeutic targets. *Nat. Rev. Nephrol.* **6**, 643–656 (2010).
- H. Okada, R. Kalluri, Cellular and molecular pathways that lead to progression and regression of renal fibrogenesis. *Curr. Mol. Med.* **5**, 467–474 (2005).
- W. A. Border, N. A. Noble, TGF- β in kidney fibrosis: A target for gene therapy. *Kidney Int.* **51**, 1388–1396 (1997).
- W. Wang, V. Koka, H. Y. Lan, Transforming growth factor- β and Smad signalling in kidney diseases. *Nephrology* **10**, 48–56 (2005).
- O. Garcia-Sánchez, F. J. López-Hernández, J. M. López-Novoa, An integrative view on the role of TGF- β in the progressive tubular deletion associated with chronic kidney disease. *Kidney Int.* **77**, 950–955 (2010).
- B. Schmierer, C. S. Hill, TGF β -SMAD signal transduction: Molecular specificity and functional flexibility. *Nat. Rev. Mol. Cell Biol.* **8**, 970–982 (2007).
- C.-H. Heldin, K. Miyazono, P. ten Dijke, TGF- β signalling from cell membrane to nucleus through SMAD proteins. *Nature* **390**, 465–471 (1997).
- J. Massagué, TGF- β signal transduction. *Annu. Rev. Biochem.* **67**, 753–791 (1998).
- C. E. Ruan, H. W. Schnaper, A.-C. Poncellet, The phosphatidylinositol 3-kinase/Akt pathway enhances Smad3-stimulated mesangial cell collagen I expression in response to transforming growth factor- β 1. *J. Biol. Chem.* **279**, 2632–2639 (2004).
- B. Hu, Z. Wu, S. H. Phan, Smad3 mediates transforming growth factor- β -induced α -smooth muscle actin expression. *Am. J. Respir. Cell Mol. Biol.* **29**, 397–404 (2003).
- H. Peinado, M. Quintanilla, A. Cano, Transforming growth factor β -1 induces snail transcription factor in epithelial cell lines: Mechanisms for epithelial mesenchymal transitions. *J. Biol. Chem.* **278**, 21113–21123 (2003).
- X. Yang, J. J. Letterio, R. J. Lechleider, L. Chen, R. Hayman, H. Gu, A. B. Roberts, C. Deng, Targeted disruption of SMAD3 results in impaired mucosal immunity and diminished T cell responsiveness to TGF- β . *EMBO J.* **18**, 1280–1291 (1999).
- A. B. Roberts, F. Tian, S. D. Byfield, C. Stuelten, A. Ooshima, S. Saika, K. C. Flanders, Smad3 is key to TGF- β -mediated epithelial-to-mesenchymal transition, fibrosis, tumor suppression and metastasis. *Cytokine Growth Factor Rev.* **17**, 19–27 (2006).
- T. R. Mercer, M. E. Dinger, J. S. Mattick, Long non-coding RNAs: Insights into functions. *Nat. Rev. Genet.* **10**, 155–159 (2009).
- M. Huarte, The emerging role of lncRNAs in cancer. *Nat. Med.* **21**, 1253–1261 (2015).
- S. Uchida, S. Dimmeler, Long noncoding RNAs in cardiovascular diseases. *Circ. Res.* **116**, 737–750 (2015).
- J. A. Briggs, E. J. Wolvetang, J. S. Mattick, J. L. Rinn, G. Barry, Mechanisms of long non-coding RNAs in mammalian nervous system development, plasticity, disease, and evolution. *Neuron* **88**, 861–877 (2015).
- J. M. Lorenzen, T. Thum, Long noncoding RNAs in kidney and cardiovascular diseases. *Nat. Rev. Nephrol.* **12**, 360–373 (2016).
- Q. Zhou, X. R. Huang, J. Yu, X. Yu, H. Y. Lan, Long noncoding RNA *Arid2-IR* is a novel therapeutic target for renal inflammation. *Mol. Ther.* **23**, 1034–1043 (2015).
- J. Long, S. S. Badal, Z. Ye, Y. Wang, B. A. Ayanga, D. L. Galvan, N. H. Green, B. H. Chang, P. A. Overbeek, F. R. Danesh, Long noncoding RNA *Tug1* regulates mitochondrial bioenergetics in diabetic nephropathy. *J. Clin. Invest.* **126**, 4205–4218 (2016).
- K. C. Pang, M. C. Frith, J. S. Mattick, Rapid evolution of noncoding RNAs: Lack of conservation does not mean lack of function. *Trends Genet.* **22**, 1–5 (2006).
- T. B. Nesterova, S. Ya. Slobodyanyuk, E. A. Elisaphenko, A. I. Shevchenko, C. Johnston, M. E. Pavlova, I. B. Rogozin, N. N. Kolesnikov, N. Brockdorff, S. M. Zakian, Characterization of the genomic *Xist* locus in rodents reveals conservation of overall gene structure and tandem repeats but rapid evolution of unique sequence. *Genome Res.* **11**, 833–849 (2001).
- J. Casper, A. S. Zweig, C. Villarreal, C. Tyner, M. L. Speir, K. R. Rosenbloom, B. J. Raney, C. M. Lee, B. T. Lee, D. Karolchik, A. S. Hinrichs, M. Haussler, L. Gurusvaidoo, J. Navarro Gonzalez, D. Gibson, I. T. Fiddes, C. Eisenhart, M. Diekhans, H. Clawson, G. P. Barber, J. Armstrong, D. Haussler, R. M. Kuhn, W. J. Kent, The UCSC Genome Browser database: 2018 update. *Nucleic Acids Res.* **46**, D762–D769 (2018).
- D. L. Wheeler, D. M. Church, S. Federhen, A. E. Lash, T. L. Madden, J. U. Pontius, G. D. Schuler, L. M. Schriml, E. Sequeira, T. A. Tatusova, L. Wagner, Database resources of the National Center for Biotechnology. *Nucleic Acids Res.* **31**, 28–33 (2003).
- A. Khan, O. Fornes, A. Stigliani, M. Gheorghe, J. A. Castro-Mondragon, R. van der Lee, A. Bessy, J. Chêneby, S. R. Kulkarni, G. Tan, D. Baranasic, D. J. Arenillas, A. Sandelin, K. Vandepoele, B. Lenhard, B. Ballester, W. W. Wasserman, F. Parcy, A. Mathelier, JASPAR 2018: Update of the open-access database of transcription factor binding profiles and its web framework. *Nucleic Acids Res.* **46**, D260–D266 (2018).
- M. Zuker, Mfold web server for nucleic acid folding and hybridization prediction. *Nucleic Acids Res.* **31**, 3406–3415 (2003).
- I. L. Hofacker, Vienna RNA secondary structure server. *Nucleic Acids Res.* **31**, 3429–3431 (2003).
- M. Kretzschmar, J. Doody, I. Timokhina, J. Massagué, A mechanism of repression of TGF β /Smad signaling by oncogenic Ras. *Genes Dev.* **13**, 804–816 (1999).
- X. Wei, Y. Xia, F. Li, Y. Tang, J. Nie, Y. Liu, Z. Zhou, H. Zhang, F. F. Hou, Kindlin-2 mediates activation of TGF- β /Smad signaling and renal fibrosis. *J. Am. Soc. Nephrol.* **24**, 1387–1398 (2013).
- T. Tsukazaki, T. A. Chiang, A. F. Davison, L. Attisano, J. L. Wrana, SARA, a FYVE domain protein that recruits Smad2 to the TGF β receptor. *Cell* **95**, 779–791 (1998).
- J. Ai, J. Nie, J. He, Q. Guo, M. Li, Y. Lei, Y. Liu, Z. Zhou, F. Zhu, M. Liang, Y. Cheng, F. F. Hou, GQ5 hinders renal fibrosis in obstructive nephropathy by selectively inhibiting TGF- β -induced Smad3 phosphorylation. *J. Am. Soc. Nephrol.* **26**, 1827–1838 (2015).
- H. Y. Lan, W. Mu, N. Tomita, X. R. Huang, J. H. Li, H.-J. Zhu, R. Morishita, R. J. Johnson, Inhibition of renal fibrosis by gene transfer of inducible Smad7 using ultrasound-microbubble system in rat UUO model. *J. Am. Soc. Nephrol.* **14**, 1535–1548 (2003).
- J. H. Li, H.-J. Zhu, X. R. Huang, K. N. Lai, R. J. Johnson, H. Y. Lan, Smad7 inhibits fibrotic effect of TGF- β on renal tubular epithelial cells by blocking Smad2 activation. *J. Am. Soc. Nephrol.* **13**, 1464–1472 (2002).
- P. Kavsak, R. K. Rasmussen, C. G. Causing, S. Bonni, H. Zhu, G. H. Thomsen, J. L. Wrana, Smad7 binds to Smurf2 to form an E3 ubiquitin ligase that targets the TGF β receptor for degradation. *Mol. Cell* **6**, 1365–1375 (2000).
- C.-C. Hou, W. Wang, X. R. Huang, P. Fu, T.-H. Chen, D. Sheikh-Hamad, H. Y. Lan, Ultrasound-microbubble-mediated gene transfer of inducible Smad7 blocks transforming growth factor- β signaling and fibrosis in rat remnant kidney. *Am. J. Pathol.* **166**, 761–771 (2005).
- H. Y. Lan, Diverse roles of TGF- β /Smads in renal fibrosis and inflammation. *Int. J. Biol. Sci.* **7**, 1056–1067 (2011).
- R. L. Chevalier, M. S. Forbes, B. A. Thornhill, Ureteral obstruction as a model of renal interstitial fibrosis and obstructive nephropathy. *Kidney Int.* **75**, 1145–1152 (2009).
- K. Zhang, X. Han, Z. Zhang, L. Zheng, Z. Hu, Q. Yao, H. Cui, G. Shu, M. Si, C. Li, Z. Shi, T. Chen, Y. Han, Y. Chang, Z. Yao, T. Han, W. Hong, The liver-enriched lnc-LFAR1 promotes liver fibrosis by activating TGF β and notch pathways. *Nat. Commun.* **8**, 144 (2017).
- M. N. Cabili, C. Trapnell, L. Goff, M. Koziol, B. Tazon-Vega, A. Regev, J. L. Rinn, Integrative annotation of human large intergenic noncoding RNAs reveals global properties and specific subclasses. *Genes Dev.* **25**, 1915–1927 (2011).
- J. Krol, I. Krol, C. P. P. Alvarez, M. Fiscella, A. Hierlemann, B. Roska, W. Filipowicz, A network comprising short and long noncoding RNAs and RNA helicase controls mouse retina architecture. *Nat. Commun.* **6**, 7305 (2015).
- R. Micheletti, I. Plaisance, B. J. Abraham, A. Sarre, C.-C. Ting, M. Alexanian, D. Maric, D. Maison, M. Nemir, R. A. Young, B. Schroen, A. González, S. Ounzain, T. Pedrazzini, The long noncoding RNA *Wisper* controls cardiac fibrosis and remodeling. *Sci. Transl. Med.* **9**, eaai9118 (2017).
- L. Ni, M. Saleem, P. W. Mathieson, Podocyte culture: Tricks of the trade. *Nephrology* **17**, 525–531 (2012).
- J. Yang, C. Dai, Y. Liu, Hepatocyte growth factor gene therapy and angiotensin II blockade synergistically attenuate renal interstitial fibrosis in mice. *J. Am. Soc. Nephrol.* **13**, 2464–2477 (2002).
- K. M. Park, J.-Y. Byun, C. Kramers, J. I. Kim, P. L. Huang, J. V. Bonventre, Inducible nitric-oxide synthase is an important contributor to prolonged protective effects of ischemic preconditioning in the mouse kidney. *J. Biol. Chem.* **278**, 27256–27266 (2003).
- J. Floege, F. Eitner, Current therapy for IgA nephropathy. *J. Am. Soc. Nephrol.* **22**, 1785–1794 (2011).
- C. Dai, J. Yang, Y. Liu, Single injection of naked plasmid encoding hepatocyte growth factor prevents cell death and ameliorates acute renal failure in mice. *J. Am. Soc. Nephrol.* **13**, 411–422 (2002).

51. C. J. Rocca, S. N. Ur, F. Harrison, S. Cherqui, rAAV9 combined with renal vein injection is optimal for kidney-targeted gene delivery: Conclusion of a comparative study. *Gene Ther.* **21**, 618–628 (2014).
52. B. Liu, L. Sun, Q. Liu, C. Gong, Y. Yao, X. Lv, L. Lin, H. Yao, F. Su, D. Li, M. Zeng, E. Song, A cytoplasmic NF- κ B interacting long noncoding RNA blocks I κ B phosphorylation and suppresses breast cancer metastasis. *Cancer Cell* **27**, 370–381 (2015).
53. F. Yu, H. Yao, P. Zhu, X. Zhang, Q. Pan, C. Gong, Y. Huang, X. Hu, F. Su, J. Lieberman, E. Song, *let-7* regulates self renewal and tumorigenicity of breast cancer cells. *Cell* **131**, 1109–1123 (2007).
54. L. Wang, T. Lyerla, Histochemical and cellular changes accompanying the appearance of lung fibrosis in an experimental mouse model for Hermansky Pudlak syndrome. *Histochem. Cell Biol.* **134**, 205–213 (2010).
55. M. Ots, H. S. Mackenzie, J. L. Troy, H. G. Rennke, B. M. Brenner, Effects of combination therapy with enalapril and losartan on the rate of progression of renal injury in rats with 5/6 renal mass ablation. *J. Am. Soc. Nephrol.* **9**, 224–230 (1998).
56. L. Raij, S. Azar, W. Keane, Mesangial immune injury, hypertension, and progressive glomerular damage in Dahl rats. *Kidney Int.* **26**, 137–143 (1984).
57. H. Trimarchi, J. Barratt, D. C. Cattran, H. T. Cook, R. Coppo, M. Haas, Z.-H. Liu, I. S. D. Roberts, Y. Yuzawa, H. Zhang, J. Feehally; IgAN Classification Working Group of the International IgA Nephropathy Network and the Renal Pathology Society, Oxford classification of IgA nephropathy 2016: An update from the IgA Nephropathy Classification Working Group. *Kidney Int.* **91**, 1014–1021 (2017).
58. D. Zhou, Y. Li, L. Lin, L. Zhou, P. Igarashi, Y. Liu, Tubule-specific ablation of endogenous β -catenin aggravates acute kidney injury in mice. *Kidney Int.* **82**, 537–547 (2012).
59. A. S. Levey, L. A. Stevens, C. H. Schmid, Y. L. Zhang, A. F. Castro III, H. I. Feldman, J. W. Kusek, P. Eggers, F. Van Lente, T. Greene, J. Coresh, A new equation to estimate glomerular filtration rate. *Ann. Intern. Med.* **150**, 604–612 (2009).
- Acknowledgments:** We thank H.-Y. Lan, L. Racusen, and M. Saleem for providing cultured cells for this study. **Funding:** This study was supported by the National Key Technology Support Program of China (2013BAI09B06 to F.F.H.), the State Key Program of National Natural Science Foundation of China (81430016 to F.F.H.), the Major International (Regional) Joint Research Project of National Natural Science Foundation of China (81620108003 to F.F.H.), the Foundation for Innovation Research Groups of the National Natural Science Foundation of China (81521003 to Y.L.), the National Science Foundation of China (81572890 to M.-L.L.), and Guangdong Province Key Laboratory of Malignant Tumor Epigenetics and Gene Regulation (2017B030314026 to S.N.). **Author contributions:** P.W., M.-L.L., T.M., and S.N. performed all in vitro and animal experiments. J.W. was involved in developing the human kidney disease cohort. Z.Z. handled the kidney samples. N.J. and G.W. analyzed renal biopsy samples. E.S. and Y.L. provided guidance with the experiments and edited the manuscript. F.H. designed the study and wrote the paper. **Competing interests:** The authors declare that they have no competing interests. **Data and materials availability:** All data associated with this study can be found in the paper or the Supplementary Materials. Microarray data are deposited in NCBI Gene Expression Omnibus (GEO) under accession no. GSE108554.
- Submitted 13 February 2018
Resubmitted 11 June 2018
Accepted 17 September 2018
Published 10 October 2018
10.1126/scitranslmed.aat2039
- Citation:** P. Wang, M.-L. Luo, E. Song, Z. Zhou, T. Ma, J. Wang, N. Jia, G. Wang, S. Nie, Y. Liu, F. Hou, Long noncoding RNA *lnc-TSI* inhibits renal fibrogenesis by negatively regulating the TGF- β /Smad3 pathway. *Sci. Transl. Med.* **10**, eaat2039 (2018).

Long noncoding RNA *Inc-TSI* inhibits renal fibrogenesis by negatively regulating the TGF- β /Smad3 pathway

Peng Wang, Man-Li Luo, Erwei Song, Zhanmei Zhou, Tongtong Ma, Jun Wang, Nan Jia, Guobao Wang, Sheng Nie, Youhua Liu and FanFan Hou

Sci Transl Med **10**, eaat2039.
DOI: 10.1126/scitranslmed.aat2039

A target for renal fibrosis

Transforming growth factor- β (TGF- β) is a known regulator of fibrosis but has remained difficult to target. Wang *et al.* identified a kidney-specific long noncoding RNA, *Inc-TSI*, that inhibited Smad3 activation and downstream profibrogenic gene expression in human tubular epithelial cells (TECs). Ectopic *Inc-TSI* expression in mouse TECs confirmed inhibition of TGF- β signaling, and delivery of *Inc-TSI* in unilateral ureteral obstruction and ischemic reperfusion injury-induced fibrosis models resulted in reduced renal fibrogenesis. Expression of *Inc-TSI* negatively correlated with fibrosis and renal failure in IgA nephropathy patients, raising the possibility that the lncRNA could be a potential therapeutic target.

ARTICLE TOOLS	http://stm.sciencemag.org/content/10/462/eaat2039
SUPPLEMENTARY MATERIALS	http://stm.sciencemag.org/content/suppl/2018/10/05/10.462.eaat2039.DC1
RELATED CONTENT	http://stm.sciencemag.org/content/scitransmed/10/422/eaao0475.full http://stm.sciencemag.org/content/scitransmed/9/395/eaai9118.full http://stm.sciencemag.org/content/scitransmed/9/417/eaam8475.full http://stm.sciencemag.org/content/scitransmed/10/426/eaan5174.full
REFERENCES	This article cites 59 articles, 18 of which you can access for free http://stm.sciencemag.org/content/10/462/eaat2039#BIBL
PERMISSIONS	http://www.sciencemag.org/help/reprints-and-permissions

Use of this article is subject to the [Terms of Service](#)

Science Translational Medicine (ISSN 1946-6242) is published by the American Association for the Advancement of Science, 1200 New York Avenue NW, Washington, DC 20005. 2017 © The Authors, some rights reserved; exclusive licensee American Association for the Advancement of Science. No claim to original U.S. Government Works. The title *Science Translational Medicine* is a registered trademark of AAAS.